

Preparation and characterization of PVDF hybrid membranes by embedding nanomaterials as silica gel and clay: evaluation of the removal efficiency of nickel and copper ions from water

Mustapha Chabane^{a,b,*}, Adalgisa Tavolaro^c, Francesca Russo^c, Giovanni Chiappetta^c, Benamar Dahmani^{a,b}, Alberto Figoli^{c,*}

^aLaboratory of Research on Spectrochemistry and Structural Pharmacology, Department of Chemistry, Science Faculty, University of Tlemcen, 13000 Tlemcen, Algeria, email: chabane@cuniv-naama.dz (M. Chabane)

^bDepartment of Technology, Institute of Science and Technology, University Center of Naama, Ctr Univ Naama, BP66, 45000 Naama, Algeria, email: chabane@cuniv-naama.dz (M. Chabane)

^cInstitute on Membrane Technology (ITM-CNR), via P. Bucci 17/C, 87036 Rende (CS), Italy, email: a.figoli@itm.cnr.it (A. Figoli)

Received 5 August 2021; Accepted 23 December 2021

ABSTRACT

The aim of this research is to study the effect of silica gel and montmorillonite clay (maghnite), often used as adsorbents in chemical applications, on the structure of hybrid poly(vinylidene fluoride) (PVDF) membranes. The membranes were synthesized using the precipitation-phase inversion method. In order to recognize the different structural changes of the PVDF in the samples various characterization techniques were tested, such as the contact angle, the scanning electron microscopy, the attenuated total reflectance-Fourier-transform infrared spectroscopy, porosity, measurement of pore size and measurements of hydraulic permeability. The review of the results allowed us to understand the effects of silica gel and maghnite on the PVDF membranes in terms of crystal phases transition, hydrophobic character, porosity, morphology and pure water permeability. The synthesized membranes were tested for the removal of copper and nickel from aqueous solution.

Keywords: Poly(vinylidene fluoride); Silica gel; Maghnite; Hybrid membranes; Copper; Nickel

1. Introduction

Poly(vinylidene fluoride) (PVDF) is becoming the preferred polymer for the manufacture of porous membranes, as it has excellent mechanical and thermal properties with high chemical stability. However, PVDF membranes present some drawbacks due their hydrophobic nature which cause the fouling phenomenon and consequently a decrease in water permeability [1,2]. The loading of inorganic nanoparticles into PVDF matrix structures has been a very important way to enhance the properties of PVDF/inorganic membranes. These types of membranes

have been applied in different industrial applications in the liquid effluents and oils treatments, broth fermentation concentration and lithium-ion batteries, agro-food, biomedical activities and water treatment, including various separation sieving mechanism such as microfiltration, ultrafiltration; etc [3–7]. Several PVDF hybrid membranes manufacturing techniques have been developed in recent years. The synthesized methods are based on the grafting of functional groups and/or modifications of surface properties or by adding the inorganic fillers within the polymeric membranes. Phase inversion by immersion precipitation (NIPS) is the most used method due to its

* Corresponding authors.

simplicity, less costly with low energy costs. The principle of the NIPS is to mix and dissolve the polymer in a solvent at a suitable temperature in order to form an homogenous solution, followed by casting on a support and then submerging in a coagulation bath containing a non-solvent. At this point, an exchange between solvent and non-solvent is established, this phenomenon depends on the kinetics phenomena, liquid–liquid demixing and thermodynamic equilibrium between phases. The precipitation process occurs, and the residual solvent is eventually evaporated. Typically, the porosity, pore distribution and pore size are directly related to the phase separation, mass transfer and diffusion phenomena, and thus the NIPS method efficiency depends on the operating conditions, but also on the mode of interaction between polymers, additives, solvents and non solvents [7]. PVDF has a molecular structure containing repeating units of (CF_2CH_2) with a semi-crystalline structure and several allotropic varieties, of various crystal phases (α , β , γ , δ , ϵ). Among the structural polymorphisms of PVDF, the α crystalline phase is non polar with very high energy stability and can be used for the manufacture of membranes filtration, whereas the crystalline phase β is commonly used for the manufacture of materials such as membrane sensors, due to its excellent piezoelectric and pyroelectric characteristics [7,8]. Fig. 1 shows different polymorphism structural phases of PVDF. The degree of crystallinity and the polymorphism type have an influence on the chemical, mechanical and thermal characteristic of PVDF polymer. It has been reported that the diversity of the polymorphism influences the PVDF membrane solute

interactions during the separation by ultrafiltration/microfiltration, which causes a different fouling effect. The PVDF membrane with predominant α crystalline phase is more resistant to fouling phenomenon. However, the β -phase-rich membrane has a great power of attraction towards proteins [7]. During the synthesis of composite membranes, the transitions of the amorphous and crystalline forms of PVDF are strongly linked to several parameters such as, the temperature and nature of the solvent [9]. Ma et al. [10] have studied the influence of THF and dimethylformamide (DMF) on the PVDF polymorphism. A higher percentage of β phase was found when DMF was used as solvent. However, it was deduced that the presence of two crystal phases α and β with mixture of solvents (THF/DMF), the β phase form increased with the addition of small amounts of DMF to the solvent mixture. The PVDF crystal phases transition can also be affected by the temperature and the additive and this has been highlighted by the experimental study of Fadaei et al. [11] which discovered that a transition from the crystalline phase β to α of PVDF occurs with increasing the temperature from 25°C to 60°C, and by incorporation of the additive PEG. It was found that the inclusion of PEG decreases the percentage of the β crystal phase with the predominance of the α crystal. This was explained by the formation of hydrogen bonds between the PEG and the PVDF chains, which cause interference on interactions between PVDF and aprotic solvents such as DMAc. Following this research, it was proved that chemical additives have an impact on the structural transition and modification on the conformations chains of PVDF.

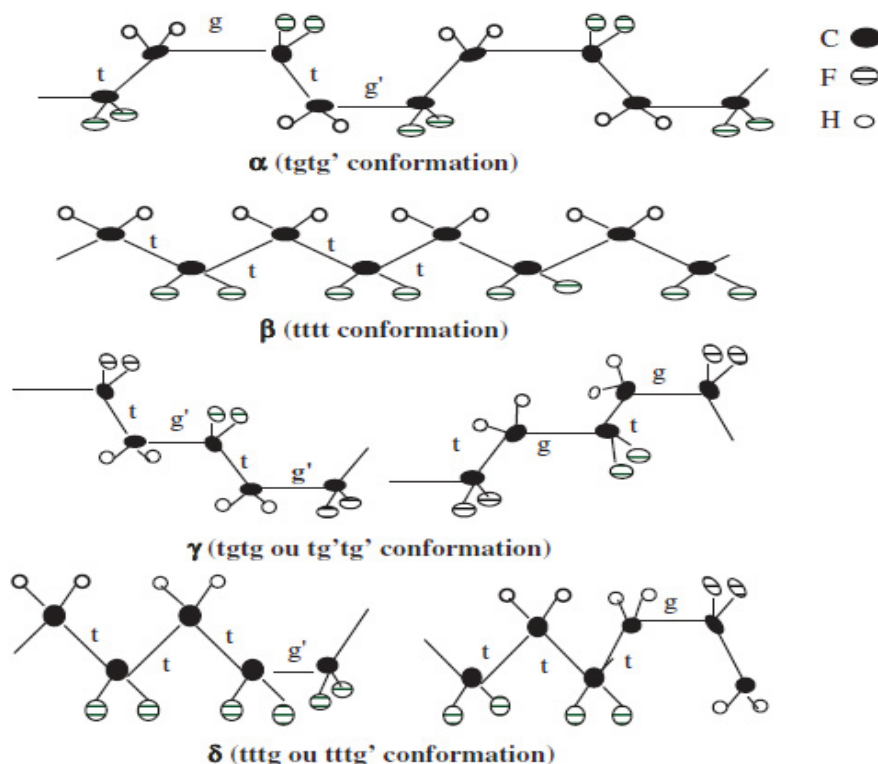


Fig. 1. Polymorphism structures of PVDF (α β γ δ conformation phases) (Reprint with permission from Belouadah et al. [12]).

Although there are different organic and inorganic compounds that can be incorporated into the polymer matrix of PVDF, the current trend is to use both additives which are found in abundance in the environment, and also improve the characteristic of the PVDF composite membranes. In this perspective, inorganic additives such as SiO_2 , TiO_2 , Al_2O_3 , ZnO , carbon nanotube have been used for the preparation of matrix hybrid membranes [3,12–16]. Considering the availability of silica in the soil, molecular structures based on silicon atoms have been highly applied as additives in the preparation of PVDF composite membrane [17]. Several researchers have studied the performance of additives based on silica for the preparation of PVDF matrix membranes. For example Zhi et al. [15] highlighted the effect of SiO_2 nanoparticles additive on the improvement of hydraulic permeability of water and the retention of BSA molecules with a significant reduction of fouling index. Ngang et al. [16] proved the hydrophilic effect of SiO_2 nanoparticles on increasing the permeate flux of the composite membrane PVDF/ SiO_2 used for oil emulsion separation. It has been proven that pore size, the porosity and the surface roughness of the membranes were increased with the addition of SiO_2 particles. Huang et al. [18] synthesized novel organic anion exchange membranes based on SiO_2 /PVDF. It has been found that the addition of silica content increased the hydrophilic character, and the water absorption, porosity and conductivity [13,19,20]. Huang et al. [18] prepared PVDF/ SiO_2 ultrafiltration membranes via inversion phase method by a tetraethoxysilane (TEOS) sol-gel process. It was observed that the crystal phase transition of PVDF (from β to α) increases when the weight ratio of TEOS reaches 20%. However, where TEOS content decreases, improvement was found in the membranes properties, in particular water permeability, hydrophilic character, porosity, pore size, herbal oil rejection. Silica nanoparticles were also present at higher contents around 60% in the composition of the natural clays. In addition, clay nanoparticles have been widely used as additives for the preparation of composite membrane PVDF/nanoclays, indeed the clays nanoparticles, are formed by silicate layered mineral nanoparticles with multiple units; that can form complex crystallizes. An individual layer unit is made up of octahedral and/or tetrahedral sheets. Octahedral sheets consist of aluminum or magnesium in sixfold coordination with the oxygen of a tetrahedral sheet and with hydroxyl. Tetrahedral sheets are made up of silicon-oxygen tetrahedra linked to tetrahedral. It was observed that the inclusion of clay nanoparticles in the polymer matrix induces structural modification of hybrid polymer-nanoparticle materials and hence the possibility of applying this composite material in different sectors such as biomedical, petrochemicals, agrofood industry and water treatment. For example, it has been found the highest performance of PVDF/montmorillonite clay nanoparticle membrane is applied in lithium ions batteries. The particularity of the montmorillonite is the geometrical multilayer structure with interleaved spaces for water adsorption, which gives hydrophilic character and represents a real motivation for incorporating these nanoparticles with hydrophilic properties for the reduction of the contact angles of PVDF/nanoclay hybrid membranes [6,21]. Morihama

and Mierzwa [22] compared three membranes of different compositions which are poly(vinylidene fluoride) (PVDF), (PVDF-nanoclay and PVDF-PVP-nanoclay), respectively. These membranes were synthesized by the phase inversion method. The PVDF mass ratio is 18%, n-methylpyrrolidone and water are used as solvent and non-solvent. The results showed that by adding nanoparticles, the permeate flux increased by 4% ($0.9130 \text{ m}^3 \text{ m}^{-2} \text{ h}^{-1} \text{ MPa}^{-1}$), while the contact angle decreased to 87.1° , which is relatively below the values of the contact angles of the other membranes. Scanning electron microscopy has shown that the presence of a dense structure containing micropores and macropores, is also related to the addition of PVP as a blowing agent. The presence of PVP has a considerable influence on the morphology and the thermodynamic properties by reducing the miscibility and consequently favors the separation of the liquid-liquid phases and consequently the formation of the pores [22–24]. Chi Yan et al. [25] proved that it is possible to synthesize nanocomposite polyvinylidene fluoride (PVDF)/nanoclay membranes having very good abrasion resistance for use in the field of desalination of seawater. Fourier-transform infrared spectroscopy (FTIR) analysis also showed a transition from the crystalline phase of PVDF from alpha to beta, the inclusion of nanoparticles allowed an alteration of PVDF structures and improved mechanical properties in terms of stiffness and reduced hydraulic permeability of the water and this following the addition of 1% by weight of nanoparticles of clays [25]. Pramono et al. [26] have synthesized different types PVDF/nanoclay using different clays, for example, montmorillonite-MMT, bentonite-BNT and cloisite 15A-CLS as additives. The characterization showed an increase of the contact angles compared to PVDF membrane, without fillers, with the possibility of using these membranes in the ultrafiltration field.

In Algeria, there is a montmorillonite-type clay called maghnite (Mag) which is found in abundance in the region of Maghnia, and it is provided by the company ENOF (Algeria). The chemical composition results of maghnite are given in Figs. 2 and 3. The maghnite is widely used as catalyst, adsorbent in water treatment and its composition is based on alumino silicate [$\text{Al}_2\text{O}_3 (\text{SiO}_2)_2 (\text{H}_2\text{O})_2$] [27].

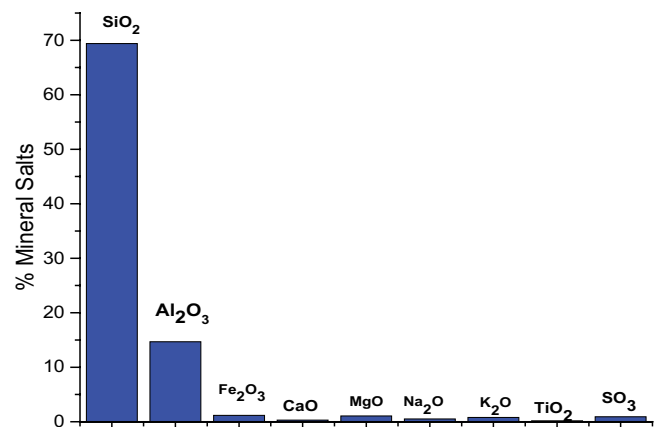


Fig. 2. Percentage of mineral salts components of maghnite clay (Adapted from Medjdoub and Mohammed [27]).

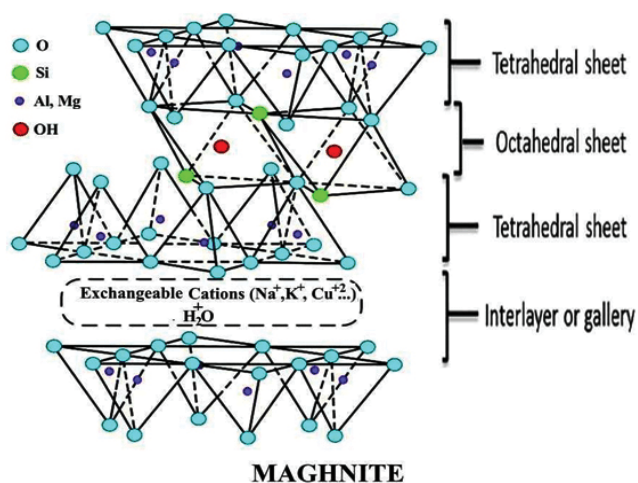


Fig. 3. General structure of montmorillonite (maghnite) clay (Adapted from Mukasa-Tebandeké et al. [28]).

The tetrahedral structure of silicon in SiO_2 has a significant influence on the properties of hybrid PVDF membranes, due to the presence of SiO bonds. However, it would be more interesting to test the effect of SiOH structure on the properties of PVDF membranes and its impact on morphology, porosity, pore size and contact angle. Silicon may also be bound to other bonds such as functional OH groups outside the crystal. Silica gel (SG) is considered as an inorganic compound which possesses these properties of presence of OH group on its surface, known by its stability, physical resistance and easy-to-control structural parameters [27]. The presence of OH groups on a silica gel surface promotes the formation of hydrogen bonds and in some cases promotes the condensation process to form siloxanes with other SG nanoparticles [29,30]. However, the presence of OH groups on the surface of silica gel promotes chemical reactivity with other functional groups [31]. Silica gel is widely used as adsorbent in several researches [32]. The other internal leaches in the crystal include the nucleus of silicon atoms bonded to oxygen atoms by siloxane (Si–O–Si). It was found that the polar properties are due to the multiple presence of residual hydroxyl groups at the surface. The number of hydroxyl groups bonded to the silicon atoms depends essentially on the number of siloxane bonds. These properties can represent a real motivation for the use of the silica gel as in hybrid membranes based on PVDF, in order to improve the hydrophilic characteristics, increase the hydraulic permeability and have information on the crystalline phase changes of the PVDF. The data collected from the literature show that the silica gel synthesized by the sol–gel method has a good reactivity by preventing the accumulation of PVDF, with possibility of PVDF chains to create links with the solvents mixtures butyrolactone (GHB) and dimethylformamide (DMF). It has been found that the PVDF nanoparticles incorporated into the SG structures modify the hydrophilic character of the SG [33]. Silica gel has also been used in the synthesis of forward osmosis (FO) membranes. For example, the characteristics of silica gel as a very hydrophilic agent and different

porosity allowed Lee et al. [34] to synthesize FO membranes based on silica gel and polyacrylonitrile. The same authors found that by using silica gel with nominal pore size in the range from 4 to 30 nm, the water permeability changed considerably with the increase of the pore size up to 9 nm for a mass percentage of silica gel, ranging from 0.25% to 1.0% [35]. Due to the excellent performance of silica gel and clay on the removal by adsorption of heavy metals from water, the interest is to use PVDF matrix membranes containing additives such as silica gel and/or clay for the decontamination of water from heavy metals such as copper and nickel ions.

The aim of this research is the synthesis and characterization of different types of PVDF, PVDF/PVP, PVDF/PVP/silica gel and PVDF/PVP/maghnite membranes for evaluating the effects of silica gel and silica combined in clay on morphology, physical–chemical properties, water permeability and the rejection of copper and nickel ions.

2. Materials and methods

2.1. Materials

The technical and commercial data of reagents and chemicals used for the synthesis and characterization of hybrid membranes are reported in Table 1.

2.2. Membrane preparation

Solvent-induced phase separation (NIPS) method is applied for synthesized PVDF membranes. The reagents proportions used for the membrane synthesis are noted in Table 2.

The homogenous PVDF solution in DMF as a polar aprotic solvent was achieved at 50°C after 24 h and cast using a casting knife (Model: Elcometer 3700 1, Germany) with a thickness of 250 μm . The membrane samples were rinsed with hot water at temperature of 60°C followed by drying in an oven at 40°C for 24 h.

3. Membrane characterization

3.1. Scanning electron microscopy

The scanning electron microscopy (SEM) analyses were performed with the EVO 10 instrument (ZEISS, Italy). The device can operate with an acceleration voltage between 200 V and 30 kV and solid-state electron detector. It can reach a resolution of 100 nm (the resolution depends on the type of sample analyzed). The top, bottom and cross-section surface were analyzed for each membrane. The samples for cross-section were frozen and fractured using nitrogen liquid.

3.2. Attenuated total reflectance/Fourier-transform infrared spectroscopy

Attenuated total reflectance-Fourier-transform infrared spectroscopy (ATR/FTIR) characterization of surface hybrid membrane samples were analyzed using PerkinElmer (Spectrum One) instrument. The instrument is equipped with ZnSe crystal/diamond system with a setting of the angle of incidence at 45° and diffusion of the order of 2 μm . The scanning number is 32 with a spectral resolution fixed at 4 cm^{-1} .

Table 1
List of reagents and chemical products

Products	Commercial name	Suppliers
Poly(vinylidene fluoride)	PVDF (Solef 6010)	Solvay (Bollate, Italy)
Polyvinylpyrrolidone	PVP (Luviskol K17)	BASF (Ludwigshafen, Germany)
Dimethylformamide	Dimethylformamide (ACS Reagent, 99.7%)	Sigma-Aldrich
Silica gel	Silica gel (99.9%, 60 Å and 250 mesh))	Sigma-Aldrich
Algerian montmorillonite	Maghnite	ENOF (Algeria)
CuCl ₂ ·2H ₂ O	Copper(II) chloride dihydrate	Sigma-Aldrich
Ni(NO ₃) ₂ ·6H ₂ O	Nickel(II) nitrate hexahydrate	Sigma-Aldrich

Table 2
Proportions of the reagents used for the membrane synthesis

Membranes	PVDF	PVP	Silica gel (SG)	Maghnite	DMF
	(wt.%)	(wt.%)	(wt.%)	(wt.%)	(wt.%)
M1	13	0	0	0	87
M2	13	2	0	0	85
A1	13	2	0.5	0	84.5
A2	13	2	1	0	84
A3	13	2	0	1	84

3.3. Porosity

Porosity was determined using gravimetric analysis and three different samples were used for each type of membranes. They were weighted before and after immersion in a wetting liquid such as Kerosene for 24 h. The porosity was determined using Eq. (1):

$$\varepsilon(\%) = \left[\frac{\frac{w_w - w_k}{\rho_k}}{\frac{w_w - w_d}{\rho_k} + \frac{w_d}{\rho_p}} \right] \times 100 \quad (1)$$

where $\varepsilon(\%)$ is the porosity percentage, w_w is the wet weight of the membrane (g), w_d is the dry weight of the membrane (g), ρ_k is the density of kerosene ($\rho_k = 0.81 \text{ g cm}^{-3}$), ρ_p is the density of PVDF polymer ($\rho_p = 1.78 \text{ g cm}^{-3}$).

3.4. Contact angle

The contact angle was assessed in static analysis by means of the sessile drop method with optical CAM100 Instrument-Tensiometer (Nordtest srl, GI, Serravalle Scrivia (AL Italy)). For each membrane, the average and standard deviation of five measurements were performed.

3.5. Pore size and pore size distribution

The tests of pore size and pore size distribution were carried out for each type of membrane using a capillary flow porometer (CFP-1500 AEXL, Porous Materials Inc., Ithaca, NY, USA). The first step consists of wetting the sample with a fluorinated liquid (Fluorinert model: FC40) for a period

of 24 h before test. The software records differences in pressures and flow rates of the gases through the membrane samples for both dry and wet states. The bubble point, mean pore size and pore fraction distribution were registered.

3.6. Experimental filtration test

The filtration experiments were carried out in a pressurized stirred filtration system of the Amicon 8200 type (Millipore, USA). The pure water permeability was determined by variation of permeate flux vs. the pressure. The retention experiment tests by membranes were established separately on solutions of CuCl₂ and Ni(NO₃)₂ with concentrations of 500 ppm of Cu and Ni.

The analysis of copper and nickel ions in feed and permeate samples were determined using atomic absorption spectrometer Analyst 400A (PerkinElmer).

The pure water permeability was calculated using Eq. (2):

$$\text{PWP} = \frac{V}{A \times t \times P} \quad (2)$$

where PWP is pure water permeability ($\text{L m}^{-2} \text{ h}^{-1} \text{ bar}^{-1}$), V is the permeate volume (L), A is the membrane area (m^2), t is the time (h), P is the difference of pressure across the membrane (bar). The pressure range was from 2 to 4 bar.

3.6.1. Rejection ratio copper and nickel ions

The rejection efficiency of nickel and copper by synthesized membranes was calculated using the following equations:

$$\% \text{ Cu rejection} = \left(1 - \frac{C_{\text{Permeate}}^{\text{Cu}}}{C_{\text{Feed}}^{\text{Cu}}} \right) \times 100 \quad (3)$$

$$\% \text{ Ni rejection} = \left(1 - \frac{C_{\text{Permeate}}^{\text{Ni}}}{C_{\text{Feed}}^{\text{Ni}}} \right) \times 100 \quad (4)$$

where % Cu rejection: percentage of copper ions rejected by synthesized membranes;

$C_{\text{Feed}}^{\text{Cu}}$: concentration of copper in permeate (ppm);

$C_{\text{Feed}}^{\text{Cu}}$: concentration of copper in feed (ppm);

% Ni rejection: percentage of nickel ions rejected by synthesized membranes;

$C_{\text{Permeate}}^{\text{Ni}}$: concentration of nickel in permeate (ppm);

$C_{\text{Feed}}^{\text{Ni}}$: concentration of nickel in feed (ppm).

4. Results and discussion

4.1. Membrane structures

In Fig. 4, SEM pictures show the morphology of the surface (top and bottom) and cross-section of the hybrid membranes. It is visible that the membrane M1, without the additives, presents a dense top and porous bottom surface (Fig. 5a and b). When the PVP was added in the dope solution, the morphology of membranes exhibits no significant differences in comparison with M1. In fact, the top layer of the M2 membrane prepared with 2 wt.% of PVP, is dense (Fig. 5d) while bottom layer is porous (Fig. 5e). The dense top layer was also observed for the A1, A2, and A3 membranes (Fig. 5g, l, o). The use of PVP increased the thermodynamic instability of casting solution and promoted the instantaneous demixing of solvent-non solvent in the coagulation bath with the formation of dense skin layer on the top surface. The cross-section of the M1 membrane highlights a porous structure with the presence of finger-like on the top (Fig. 5c). The cross section of M2 membrane exhibits the dense selective layer with the presence of macrovoids and of a porous sub-layer (Fig. 5f).

In Fig. 5 the effect of SG on the A1 (0.5 wt.% of SG) and A2 (1 wt.%) membranes with PVP is reported. The major role of SG in the membrane preparation is mainly related to its hydrophilic properties, which favor the increase of pore dimension of the membrane due to the exchange rate with DMF and water, leading to reduction of the energy between two interfaces of non-miscible solvents [10,36].

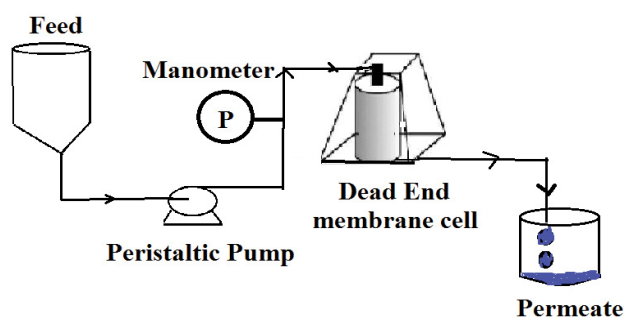


Fig. 4. Membrane filtration system.

The morphology of these membranes (A1 and A2) is similar to each other with a dense bottom surface (Fig. 5h and m, respectively) and a finger-like structure with the presence of macrovoids (Fig. 5i and n), indicating a rapid phase separation during the casting. A great difference in cross-section morphology has been observed between the PVDF/SG membranes (A1 and A2) and the PVDF/maghnite membrane (A3). When maghnite (1 wt.%) and PVP (2 wt.%) were mixed in the dope solution (A3), the morphology of the surface (top and bottom) and cross-section (Fig. 5p and q) was similar to that observed for M2 membranes. Furthermore, the cross-section of A3 (Fig. 5o) evidences that the presence of maghnite increases the selective layer on the cross-section, which is in accordance with the research based on the mixture of clay and PVDF [22,25]. It was observed that the structure of microporous layer of the hybrid blended membrane PVDF/maghnite has an effect on pure water permeability which is expected in the case of the presence of the clay in the PVDF polymeric matrix [27].

4.2. Attenuated total reflectance/Fourier-transform infrared spectroscopy

ATR/FTIR spectroscopic analysis gives the possibility to make a comparison between the functional groups present in the surfaces of the different membranes and to deduce the structural modifications of the various forms of PVDF by collecting necessary information from the literature. The identification of PVDF-based peaks has been solved by taking into account bibliographic data from some research works. The strategy of identification of the functional groups is based on a comparative study in different ranges of the wavenumbers (Figs. 6 and 7).

Table 3 reports the results of Fig. 5. The tiny trace of humidity exhibits weak symmetrical OH bands for the membranes M2 and A3. Analysis of other wavenumbers regions shows that the main vibration modes of the CH_2 and CF_2 functional groups are present in all ATR/FTIR spectra, which is explained by the predominance of PVDF in the composition of all synthesized membranes. This is shown by the symmetrical stretching, asymmetrical stretching, bending, rocking and twisting of CH_2 assigned respectively to the wavenumbers located at 3,025; 2,850; 1,430 and 946 cm^{-1} . Moreover, the coupling effects between different vibration modes of CH_2 , CF_2 , CCC and CC groups were observed, attributed to wavenumbers at 1,400; 1,276; 1,176; 1,050; 976; 946; 880; 840; 812; 796 and 765 cm^{-1} .

4.2.1. Effect of additives on the infrared bands intensities

Comparison between ATR/FTIR spectra of membrane samples reveals variation in absorption intensities and displacement effects of certain infrared bands. Indeed, Fig. 6 shows a decrease in absorption and difference in the shape of the bands situated between 1,670 to 1,675 cm^{-1} assigned to symmetric stretching band of carbonyl to PVP [32], which is used as pore-forming agent when the hybrid membranes have been prepared. The most extreme adsorption of the symmetric stretching band of C=O is due to the spectrum of the membrane M2 (13% PVDF/2% PVP); However, there is a gradual decrease in the C=O symmetric stretching bands

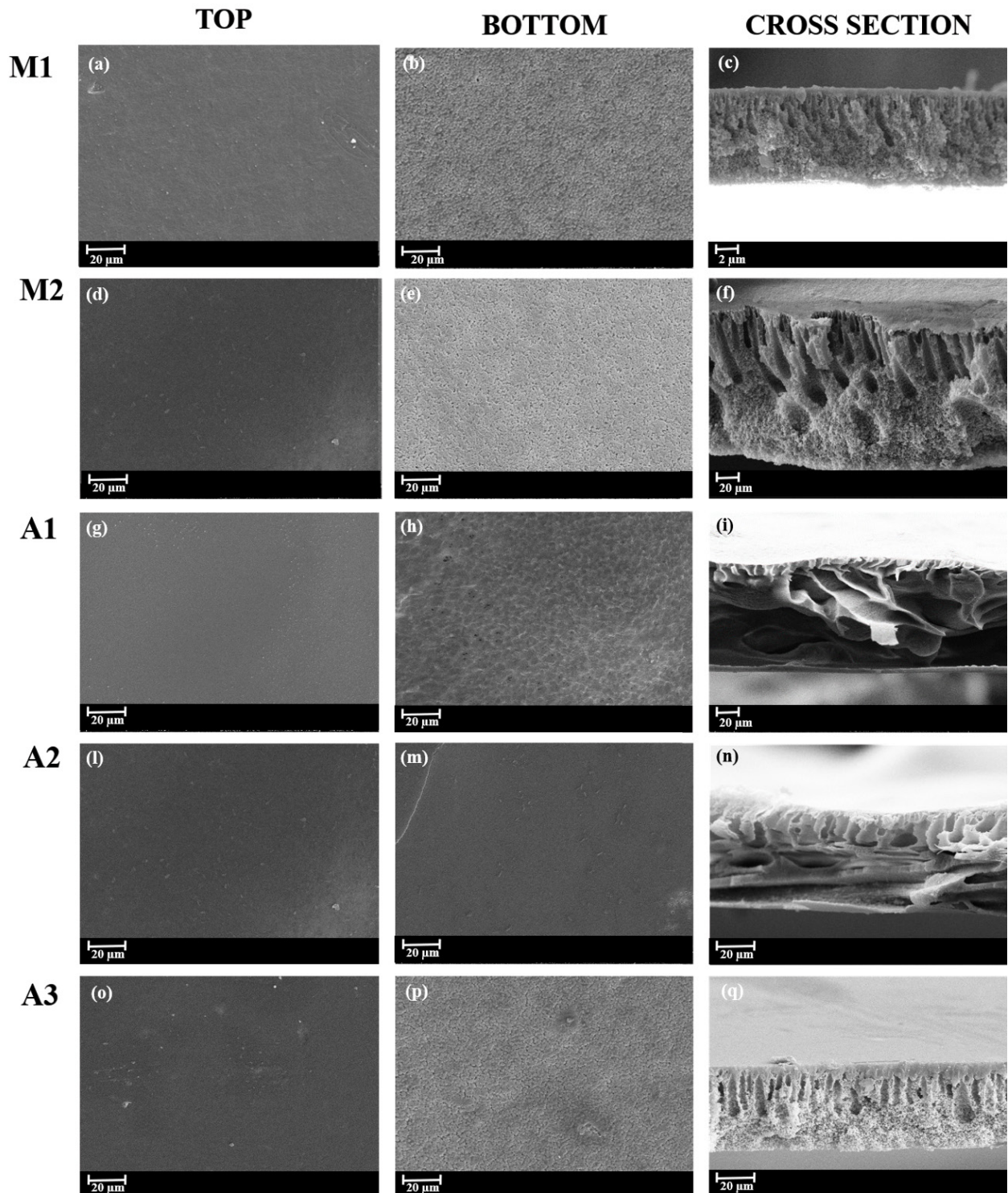


Fig. 5. SEM pictures of the hybrid PVDF membranes: (a–c) M1 (Mag 2.00 KX), (d–f) M2 (Mag 2.00 KX), (g–i) A1 (Mag 2.00 KX cross-section Mag 900 X), (l–n) A2 (Mag 2.00 KX) and (o–) A3 (Mag 2.00 KX).

absorbances for samples A1 (13% PVDF/2% PVP/0.5% SG) and A2 (13% PVDF/2% PVP/1% SG), This is explained by the effect of the increase in the amount of silica gel in the polymeric matrices and subsequently the formation of some hydrogen bonds between SG and the oxygen atoms of the

PVP carbonyl groups. The cause of disappearance of the symmetrical stretching vibration band of the C=O in the spectra of samples M1 (13% PVDF) and A3 (13% PVDF/2% PVP/1% maghnite) is also due to the absence of the carbonyl functional group in the membrane structure M1 (PVDF),

Table 3
Vibration modes of functional groups and crystalline structures of PVDF.

Wavenumbers (cm ⁻¹)					Assignment [37–40]	Crystalline	Attribution and remarks
M1	M2	A1	A2	A3			
–	3490 ^w	–	–	3500 ^w	ν_{sOH}	–	OH of H ₂ O Humidity trace Disappearance of OH bands for (M1,A1,A2)
3025 ^w	3025 ^w	3025 ^{vw}	3025 ^{vw}	3025 ^w	ν_{aCH_2}	–	CH ₂ of PVDF Less absorption intensity for (A1,A2)
2850 ^w	2920 ^w	2980 ^{vw}	2980 ^{vw}	2920 ^w	ν_{sCH_2}	–	CH ₂ of PVDF less absorption intensity for (A1,A2)
–	1675 ^w	1670 ^{vw}	1670 ^{vw}	–	$\nu_c = o$	–	C=O of PVP Disappearance of C=O Band for M1 and A3
1430 ^{vw}	1430 ^{vw}	1430 ^{vw}	1430 ^{vw}	1430 ^{vw}	δ_{CH_2}	γ [11]	CH ₂ of PVDF
1400 ^{vs}	1400 ^{vs}	1400 ^s	1400 ^s	1400 ^s	$\omega_{CH_2} - \nu_{aCC}$	α [41]	CH ₂ of PVDF CC of PVDF CC of PVP Less absorption intensity for (A1,A2,A3) compared to (M1 and M2)
1276 ^s	1276 ^s	1276 ^m	1276 ^m	1276 ^m	$\nu_{sCF_2} - \nu_{sCC} - \delta_{CCC}$	β [10] γ [11]	CF ₂ of PVDF CC of PVDF CCC of PVDF CC of PVP CCC of PVP Same remarks
1235 ^s	1235 ^s	–	–	1235 ^m	–	α [46] + γ [11]	Disappearance of band for A1 and A2
1176 ^{vs}	1176 ^{vs}	1176 ^s	1176 ^s	1176 ^s	$\nu_{aCF_2} - r_{sCF_2} r_{CH_2}$	β [10] γ [11] β [10] + γ [11]	CF ₂ of PVDF CH ₂ of PVDF CH ₂ of PVP Less absorption intensity for (A1,A2,A3) compared to (M1 and M2)
1070 ^s	1070 ^s	1070 ^m	1070 ^m	1050 ^m	$\nu_{aCC} - \omega_{CF_2} \omega_{CH_2}$ $\nu_{aSi-O-Si}$ $\nu_{aSi-O-Al(A3)}$	β [10] β [10] + γ [11] α [46] + β [10] + γ [11] α [10]	CF ₂ of PVDF CH ₂ of PVDF CH ₂ of PVP Si–O–Si Si–O–Al Decrease in absorption intensity for A1,A2,A3 compared to M1 and M2
976 ^w	–	976 ^{vw}	976 ^{vw}	–	t_{CH_2}	α [10]	CH ₂ of PVDF Disappearance of band for M2 and A3
946 ^{vw}	946 ^{vw}	946 ^{vw}	946 ^{vw}	946 ^{vw}	$t_{CH_2} + r_{CH_2}$	–	CH ₂ of PVDF
875 ^{vs}	880 ^{vs}	875 ^s	875 ^s	880 ^s	$\nu_{aCC} + \omega_{CF_2}$	β [10] β [10] + γ [11] α [46] + β [10] + γ [11] α [7] + β [10]	CF ₂ of PVDF CC of PVDF less absorption intensity for (A1,A2,A3) compared to (M1 and M2)
838 ^{vs}	838 ^{vs}	840 ^s	840 ^s	838 ^s	$\nu_{aCC} + \omega_{CF_2}$	β [10] β [10] + γ [11] γ [11]	CF ₂ of PVDF CC of PVDF PVDF less absorption intensity for (A1,A2,A3) compared to (M1 and M2)
812 ^w	–	812 ^w	812 ^w	–	r_{CH_2}	γ [13]	Disappearance of band for M2 and A3
796 ^m	796 ^m	796 ^m	796 ^m	–	r_{CH_2}	α [10]	CH ₂ of PVDF CH ₂ of PVP
765 ^w	–	765 ^w	765 ^w	–	$\delta_{CF_2} + \delta_{CCC} \nu_{sSi-O-Si(A1:A2)}$ $\nu_{sSi-O-Al(A3)}$	α [43]	CF ₂ of PVDF CC of PVDF CCC of PVDF (disappearance of band for M2 and A3)

ν_s : symmetric; ν_a , ν_s : stretching; ν_a : antisymmetric stretching; δ : bending; ω : wagging; r : rocking; t : twisting; w : weak; vw : very weak; s : strong; vs : very strong; m : medium.

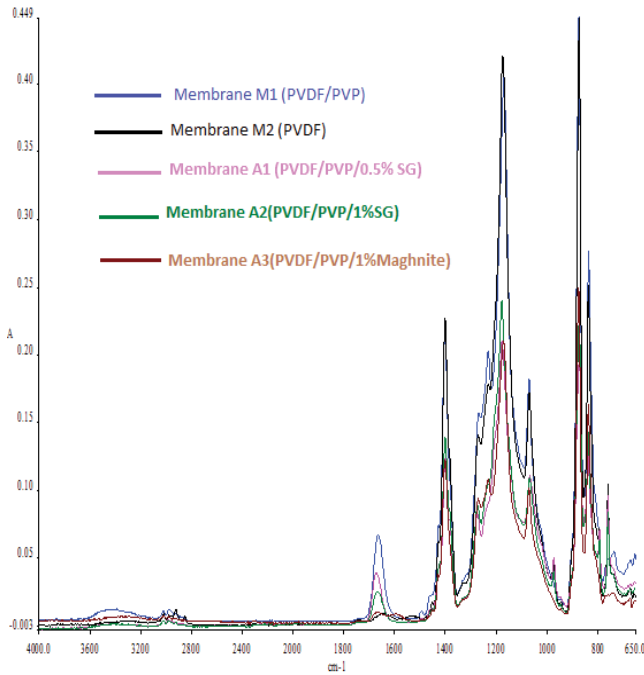


Fig. 6. Comparison between the ATR/FTIR spectra of the synthesized membranes.

and to the great numbers of bands formed between the hydrogen atoms of the montmorillonite maghnite) in the membrane A3 and the oxygen atoms of the carbonyl groups. The change in symmetric stretching C=O band is justified by different types of intermolecular and intra-molecular hydrogen bonding interactions [41]. It was also observed that the inclusion of SG and montmorillonite maghnite in the PVDF/PVP polymeric matrices results in a decrease in the absorbances at number of waves 1,400; 1,276; 1,176; 1,070 and 946 cm⁻¹, as demonstrated by the multiplication of bonds that affect the vibration modes of atomic bonds.

At the wavenumbers range situated between 1,070 and 1,050 cm⁻¹, it was remarked the reduction of the infrared absorption bands for the membranes A1 (13% PVDF/2% PVP/0.5% SG), A2 (13% PVDF/2% PVP/1% SG) and A3 (13% PVDF/2% PVP/1% maghnite). This is explained by the increasing amounts of SG in the PVDF and PVDF/PVP polymer matrix causing interference between the coupling of asymmetric stretching vibration band (CC), wagging modes (CH₂,CF₂) and the symmetrical stretching vibration band of the Si–O–Si [32,42] with the formation of hydrogen

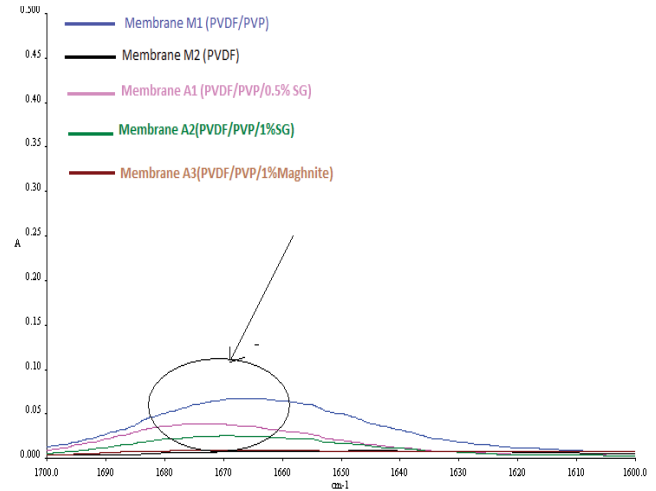


Fig. 7. Decrease in the absorption bands of the carbonyl group for each membrane.

bond between the PVDF aliphatic hydrogen and SG oxygen atoms.

4.2.2. Impact of additives on the modification of crystalline PVDF structures

As shown in Table 5 and Fig. 8, PVDF crystalline structures for each membranes have been identified using literature data [10,11,41,43]. The assignment of the infrared bands to crystalline forms α , β and/or γ is very delicate procedure, considering the hundreds of research works in this field, but also the incompatibility in the identification of crystalline structure in some typical bands [11]. However, since the two crystalline structures α and β are of particular interest to the energetic stability and pyro and piezoelectric properties and since there is an overlapping effect of several peaks in ATR/IR spectra. Individual peaks may be used for the identification and measurement of the fractions of crystalline structures [8]. The infrared bands located at 795 and 975 cm⁻¹ are attributed to α phase, and at 840 and 1,274 cm⁻¹ belong to the β phase [44].

It is possible to measure the ratio of the crystalline structure $F(\beta)$ by determination of the absorbance values of the vibration bands [8,10].

$$F(\beta) = \frac{A_{\beta}}{1.3A_{\alpha} + A_{\beta}} \tag{5}$$

Table 4
Absorbance of the carbonyl group located in the 1,600–1,700 cm⁻¹

Samples	M1	M2	A1	A2	A3
Components	PVDF	13% PVDF 2% PVP	13% PVDF 2% PVP 0.5% SG	13% PVDF 2% PVP 1% SG	13% PVDF 2% PVP 1% maghnite
Absorbance	–	0.06	0.025	0.012	–
Wavenumbers (cm ⁻¹)	–	1,675	1,670	1,670	–

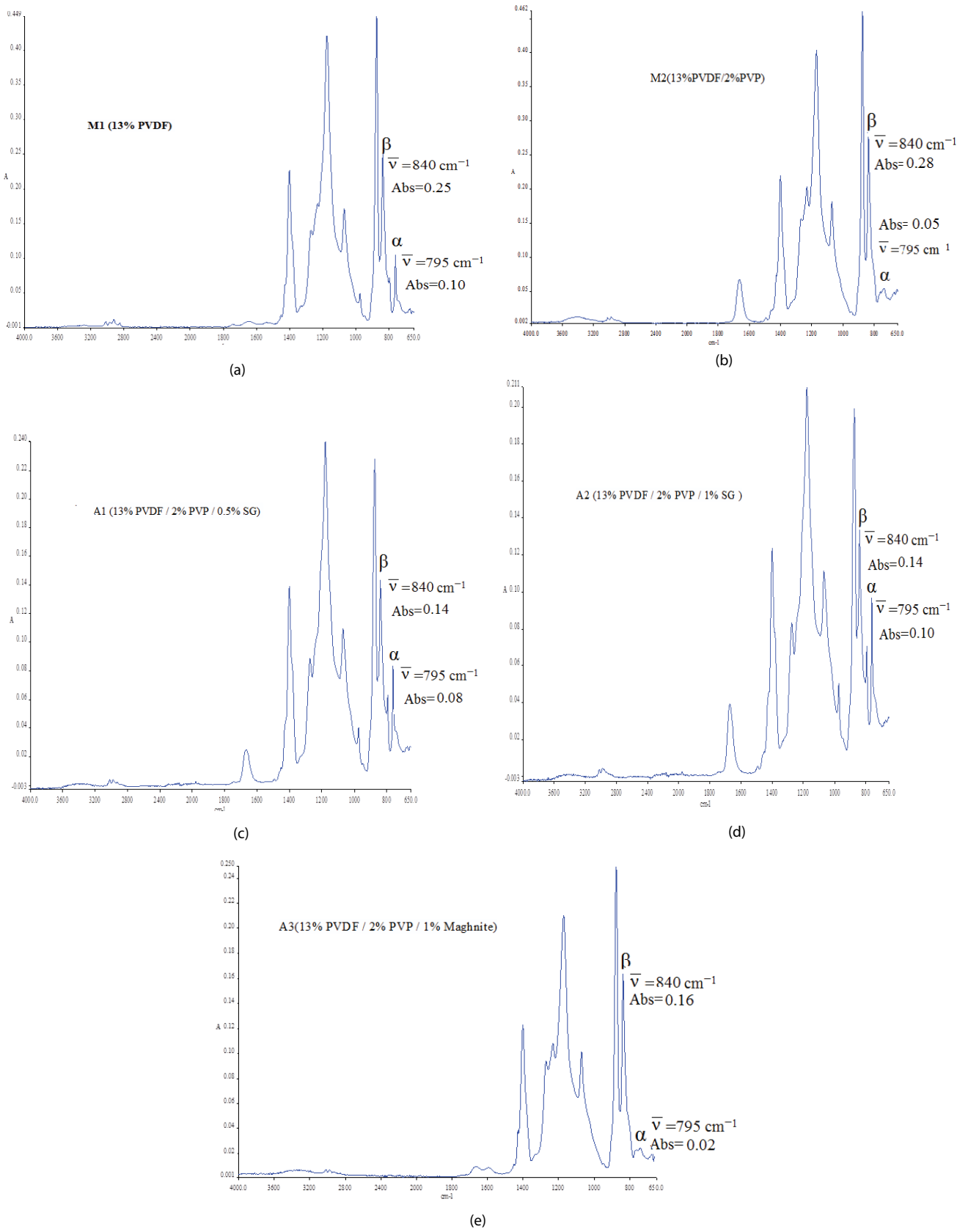


Fig. 8. Infrared bands α , β structures of PVDF for different membranes.

Table 5
Evolution of beta crystal factor for each membrane

Membranes	A_α	A_β	$F(\beta)$
M1	0.10	0.25	0.65
M2	0.05	0.28	0.80
A1	0.08	0.14	0.573
A2	0.08	0.14	0.573
A3	0.02	0.16	0.86

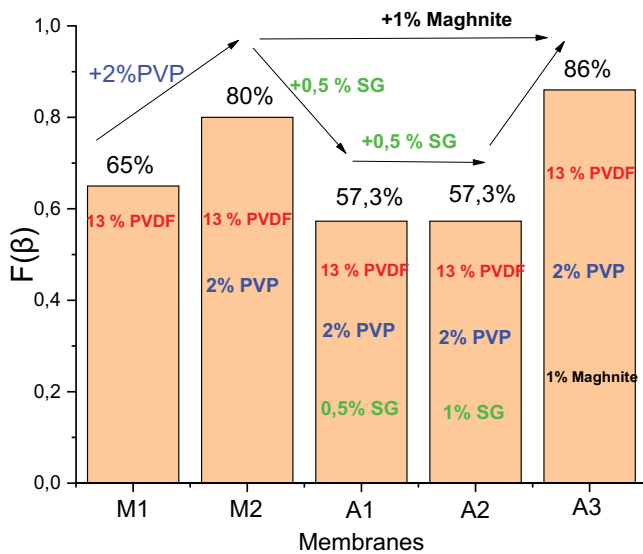


Fig. 9. β phase for M1, M2, A1, A2 and A3 membranes.

where A_α and A_β is absorption for bands situated at 795 and 840 cm^{-1} corresponding respectively to α , β conformation structures.

As shown in Fig. 9, the findings show the influence of the existence of additives on the evolution of the crystalline phase β for each membrane; While the β phase ratio for the PVDF based M1 membrane is 65%, which is due to the experimental conditions such as casting temperature of 50°C and the DMF based aprotic solvent [11,43]. However, the effect of the addition 2% of PVP increases the β phase ratio from 65% for M1 membrane to 80% for M2 membrane, explained by the significant contribution of PVP in the formation of pores and the increase of β crystalline structure previously demonstrated by study [37]. In addition, the divergence in the variance of β phase ratios for the membranes A1, A2 and A3, was noticed and this despite the addition of the amount of 0.5% SG to the composition of the polymer matrix of M2 (13% PVDF/2% PVP) for the preparation of two hybrid matrix membranes containing PVDF, PVP and SG. Moreover, β crystal phase ratio for the A1 and A2 membranes has similar value of 56.7%, which reflects a lower β phase ratio relative to the other synthesized membranes. This is justified by the SG inhibition influence on the creation of TTTT conformation structure (β phase). For the membrane A3, containing the additive montmorillonite (maghnite), the β phase ratio reaches higher value of 86%. This is due to the presence of

Table 6
Contact angle and porosity measurements

Membrane code	Porosity (%)*	Contact angle (°)	
		Air side (°)	Glass side (°)
M1	58	101	118
M2	61	72	126
A1	68	95	98
A2	63	92	96
A3	55	101	120

*Error was less than 5%.

the clay nanoparticles which promotes the crystal transition of PVDF from the α to β with increased polarity [45].

4.3. Discussion of the results for pore size, porosity and contact angle

The porosity and contact angle of the membranes are shown in Table 6. The porosity of the membranes was in the range from 55% to 68%. The PVDF membranes with SG (A1, A2) show the highest porosity (68% and 63%, respectively) with respect to the others, probably due to the presence of macrovoids in the structure. The contact angle is an important parameter to determine the wetting ability of the membranes.

The contact angle for M1 PVDF membrane (without the presence of additives) was about 100° for the top and 118° for the bottom side. The membranes showed high hydrophilic character when the PVP (72° for the top of M2) and SG (95° for the top of A1 and 92° for the top of A2) were used. The values of CA for A3, when the maghnite was added in the casting solution, was similar to A1 (101° for the top and 120° for the bottom). In all cases the dense top surface of the membranes was more hydrophilic than the bottom surface due to the presence of porous side on the bottom as confirmed by SEM analysis and in accordance with the Cassie–Baxter theory. In fact, the contact angle of the porous surface is higher than dense surface as a consequence due to the inclusion of air in the pores [6].

The results in term of largest pore size, mean flow pore size measurement are in accordance with the SEM analyses and are reported in Fig. 10. The mean flow pore diameter was 0.03 μm for M1 and M2 membranes, without and with the presence of PVP K17, respectively. The same pore size was also obtained for A3 membrane when maghnite was used. The pore size increased when SG was added in the casting solution from 0.05 μm for A2 to 0.1 μm for A1.

4.4. Pure water permeability and the rejection efficiency of copper and nickel

Fig. 11 reports the pure water permeability (PWP) and copper and nickel rejection results. It can be seen that the presence of PVP increased the PWP of the membranes from 17 $\text{L m}^{-2} \text{h}^{-1} \text{bar}^{-1}$ for M1 (without PVP) to 125 $\text{L m}^{-2} \text{h}^{-1} \text{bar}^{-1}$ for M2. The applied pressure was about 2 bar. This result is in agreement with the literature data [46,47].

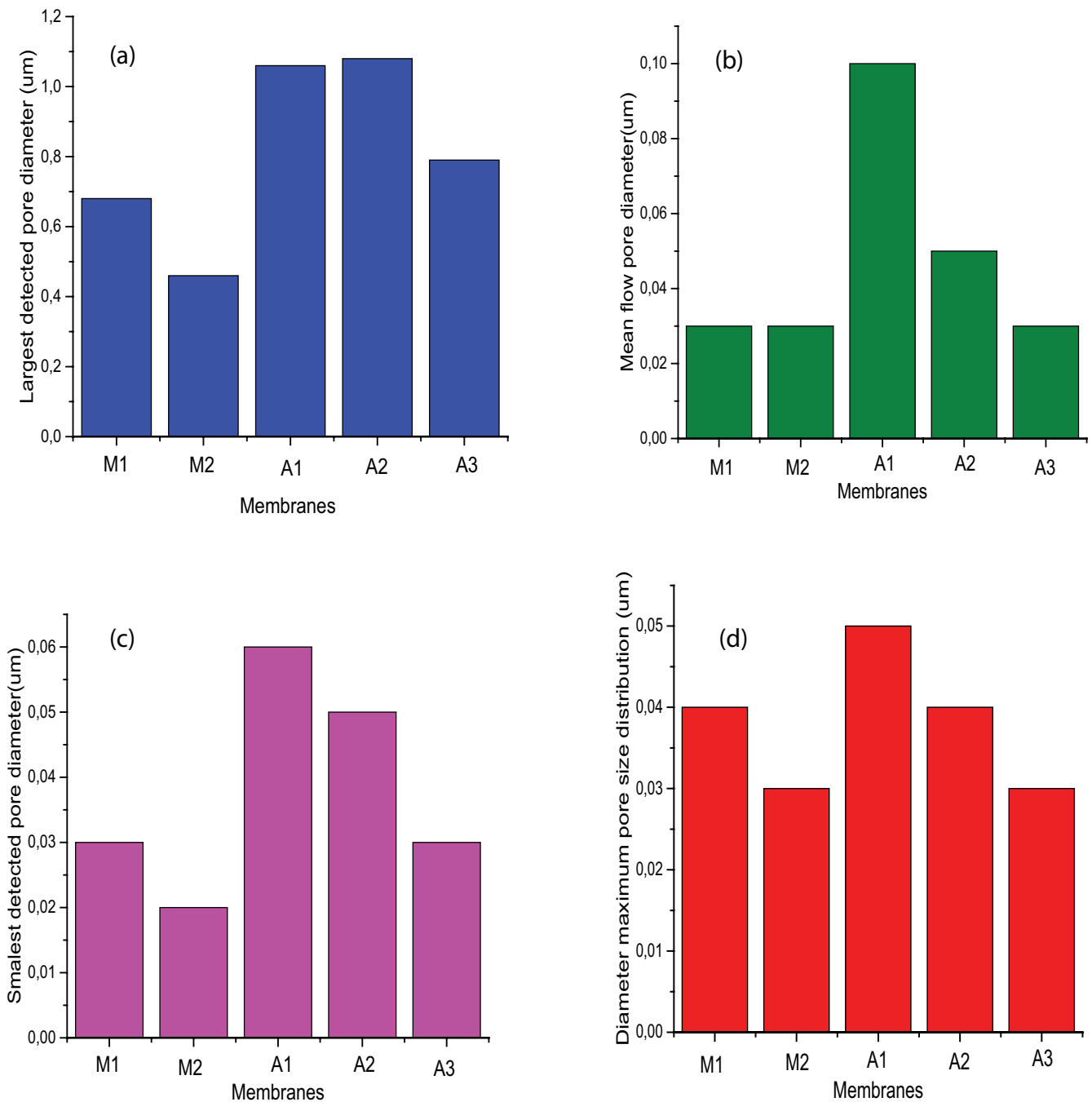


Fig. 10. Pore size measurement curves: (a) largest pore size, (b) mean flow pore size, (c) smallest pore size, and (d) diameter at maximum pore size distribution.

The A1 and A2 membranes, with different concentration of silica gel (SG), presented the highest permeability (about $450 \text{ L m}^{-2} \text{ h}^{-1} \text{ bar}^{-1}$ for A1 and $520 \text{ L m}^{-2} \text{ h}^{-1} \text{ bar}^{-1}$ for A2). This effect is justified by the inclusion of silica gel in the PVDF/PVP polymer matrix which increases the pore size and the porosity, as reported in literature [10,23].

For A3 membrane, prepared with the presence of maghnite the PWP was $90 \text{ L m}^{-2} \text{ h}^{-1} \text{ bar}^{-1}$. It was also reported in Fig. 11 the effect of SG additive amount on the increase of

rejection ratios for copper and nickel: from 27% and 25% for M1 to 47% and 42% for A2. Moreover, the high rejection ratios 55% for copper and 52% for nickel were found by membrane A3 containing 1% of maghnite clay additive. This can be justified by the effect of maghnite clay on the adsorption of heavy metals but also by the property of the β polar phase of PVDF with β phase ratio of 86% for membrane A3. This result is confirmed by previous research paper of Chabane et al. [48].

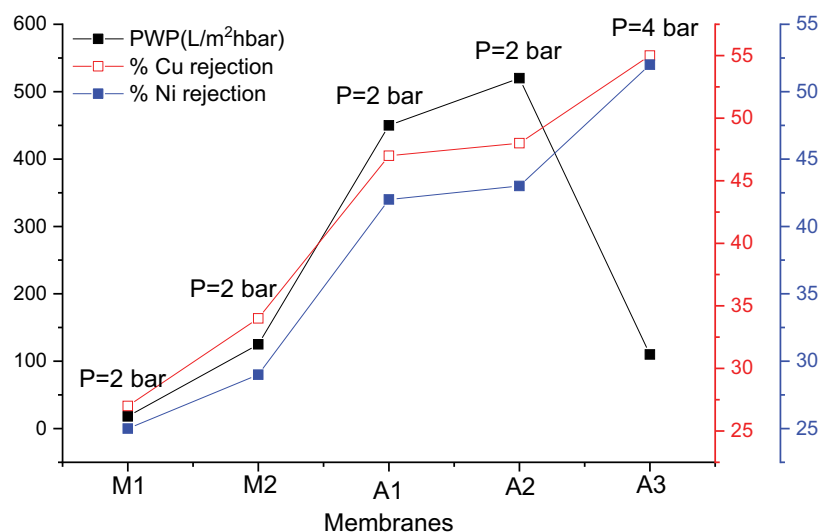


Fig. 11. PWP of membranes and rejection efficiency of copper and nickel ions at different pressures ($C_{\text{Feed}}^{\text{Cu}} = 500$ ppm, $C_{\text{Feed}}^{\text{Ni}} = 500$ ppm).

5. Conclusions

PVDF hybrid membranes were prepared by using different additives such as PVP K17, silica gel and Algerian montmorillonite (maghnite). The membranes were synthesized by NIPS techniques using DMF as solvent. It was found that the silica gel and maghnite exhibit different behaviours, as inorganic additives, incorporated with PVDF and PVP. Indeed, the effects of these additives are mainly reflected in the transitions of crystalline forms of PVDF from α and β . It has been proven that the creation of hydrogen bonds linked silica gel to PVP by preventing the latter from creating any other bond with the hydrogen of the CH group of PVDF and consequently the increase in absorbances attributed to the rocking and twisting modes corresponding to the absorbance of the α phase which causes a decrease in the crystalline factor. On the contrary, the maghnite contains more hydroxide bonds and therefore more possibilities for the creation of hydrogen bonds with the CH_2 group of PVDF and PVP. Moreover, the morphological studies proved that the membrane containing maghnite nanoclay additive presented a very dense structure compared to that with silica gel. The silica gel contributed to increased porosity, pore size and hydrophilic character of the membrane. This is confirmed by the higher values of the water permeability for the membranes containing silica gel. However, it was found that the membrane containing maghnite additive requires higher pressure of 4 bar due to dense structure. It was found also that the rejection of copper and nickel by membranes containing SG and maghnite nanoclay, is higher compared to other membranes with PVP.

References

- [1] A. Figoli, T. Marino, F. Galiano, S.S. Dorraji, E. Di Nicolò, T. He, Sustainable Route in Preparation of Polymeric Membranes, A. Figoli, A. Criscuoli, Eds., Sustainable Membrane Technology for Water and Wastewater Treatment, Part of the Green Chemistry and Sustainable Technology Book Series (GCST), Springer Nature, Switzerland, 2017, pp. 97–120.
- [2] M. Chabane, C. Melkaoui, B. Dahmani, S. Zahia Belalia, Preparation and characterization of matrix hybrid membranes poly(vinylidene fluoride)/poly(vinylpyrrolidone)/silica gel/zinc oxide for Cr(VI) removal from water, *Ann. Chim. Sci. Des. Mater.*, 44 (2020) 311–318.
- [3] S.-i. Sawada, C. Ursino, F. Galiano, S. Simone, E. Drioli, A. Figoli, Effect of citrate-based non-toxic solvents on poly(vinylidene fluoride) membrane preparation *via* thermally induced phase separation, *J. Membr. Sci.*, 493 (2015) 232–242.
- [4] T. Marino, F. Russo, A. Figoli, The formation of poly(vinylidene fluoride) membranes with tailored properties via vapour/non-solvent induced phase separation, *Membranes (Basel)*, 8 (2018) 71, doi: 10.3390/membranes8030071.
- [5] O. Benhabiles, F. Galiano, T. Marino, H. Mahmoudi, H. Lounici, A. Figoli, Preparation and characterization of TiO_2 -PVDF/PMMA blend membranes using an alternative non-toxic solvent for uf/mf and photocatalytic application, *Molecules*, 24 (2019) 724, doi: 10.3390/molecules24040724.
- [6] J.C. Barbosa, J.P. Dias, S. Lanceros-Méndez, C.M. Costa, Recent advances in poly(vinylidene fluoride) and its copolymers for lithium-ion battery separators, *Membranes*, 8 (2018) 45, doi: 10.3390/membranes8030045.
- [7] X.M. Tan, D. Rodrigue, A review on porous polymeric membrane preparation. Part I: production techniques with polysulfone and poly(vinylidene fluoride), *Polymers*, 11 (2019) 1160, doi: 10.3390/polym11071160.
- [8] N. Ideris, A.L. Ahmad, B.S. Ooi, S.C. Low, Correlation study of PVDF membrane morphology with protein adsorption: quantitative analysis by FTIR/ATR technique, *IOP Conf. Ser.: Mater. Sci. Eng.*, 358 (2018) 012054, doi: 10.1088/1757-899X/358/1/012054.
- [9] F. Guo, S. Aryana, Y. Han, Y. Jiao, A review of the synthesis and applications of polymer–nanoclay composites, *Appl. Sci.*, 8 (2018) 1696, doi: 10.3390/app8091696.
- [10] W. Ma, J. Zhang, S. Chen, X. Wang, Crystalline phase formation of poly(vinylidene fluoride) from tetrahydrofuran/*N,N*-dimethylformamide mixed solutions, *J. Macromol. Sci. Part B Phys.*, 47 (2008) 434–449.
- [11] A. Fadaei, A. Salimi, M. Mirzataheri, Structural elucidation of morphology and performance of the PVDF/PEG membrane, *J. Polym. Res.*, 21 (2014) 1–8.
- [12] R. Belouadah, D. Kendil, E. Bousbiat, D. Guyomar, B. Guiffard, Electrical properties of two-dimensional thin films of the ferroelectric material poly(vinylidene fluoride) as a function of electric field, *Physica B*, 404 (2009) 1746–1751.
- [13] X. Zhang, J. Zhou, X. Zou, Z. Wang, Y. Chu, S. Wang, Preparation of nano- $\text{SiO}_2/\text{Al}_2\text{O}_3/\text{ZnO}$ -blended PVDF cation-exchange

- membranes with improved membrane permselectivity and oxidation stability, *Materials (Basel)*, 11 (2018) 2465, doi: 10.3390/ma11122465.
- [14] H. Razzaq, H. Nawaz, A. Siddiq, M. Siddiq, S. Qaisar, A brief review on nanocomposites based on PVDF with nanostructured TiO₂ as filler, *Madridge J. Nanotechnol. Nanosci.*, 1 (2016) 23–29.
- [15] S.-H. Zhi, J. Xu, R. Deng, L.-S. Wan, Z.-K. Xu, Poly(vinylidene fluoride) ultrafiltration membranes containing hybrid silica nanoparticles: preparation, characterization and performance, *Polymer*, 55 (2014) 1333–1340.
- [16] H.P. Ngang, A.L. Ahmad, S.C. Low, B.S. Ooi, Preparation of PVDF/SiO₂ composite membrane for salty oil emulsion separation: physicochemical properties changes and its impact on fouling propensity, *IOP Conf. Ser.: Mater. Sci. Eng.*, 206 (2017) 012083.
- [17] M.O. Mavukkandy, M.R. Bilad, J. Kujawa, S. Al-Gharabli, H.A. Arafat, On the effect of fumed silica particles on the structure, properties and application of PVDF membranes, *Sep. Purif. Technol.*, 187 (2017) 365–373.
- [18] X. Huang, J. Zhang, W. Wang, Y. Liu, Z. Zhang, L. Li, W. Fan, Effects of PVDF/SiO₂ hybrid ultrafiltration membranes by sol-gel method for the concentration of fennel oil in herbal water extract, *RSC Adv.*, 5 (2015) 18258–18266.
- [19] X. Zuo, S. Yu, X. Xu, J. Xu, R. Bao, X. Yan, New PVDF organic-inorganic membranes: the effect of SiO₂ nanoparticles content on the transport performance of anion-exchange membranes, *J. Membr. Sci.*, 340 (2009) 206–213.
- [20] W. Wang, X. Chen, C. Zhao, B. Zhao, H. Dong, S. Ma, L. Li, L. Chen, B. Zhang, Cross-flow catalysis behavior of a PVDF/SiO₂@Ag nanoparticles composite membrane, *Polymers*, 10 (2018) 59, doi: 10.3390/polym10010059.
- [21] H.-Y. Hwang, D.-J. Kim, H.-J. Kim, Y.-T. Hong, S.-Y. Nam, Effect of nanoclay on properties of porous PVDF membranes, *Trans. Nonferrous Met. Soc. China*, 21 (2011) s141–s147.
- [22] A.C.D. Morihama, J.C. Mierzwa, Clay nanoparticles effects on performance and morphology of poly(vinylidene fluoride) membranes, *Braz. J. Chem. Eng.*, 31 (2014) 79–93.
- [23] Y.X. Ma, F.M. Shi, M.N. Wu, J. Ma, Effect of additives in the casting solutions on the morphology and performance of PVDF membranes, *Adv. Mater. Res.*, 391–392 (2012) 1412–1416.
- [24] M. Nasir, H. Matsumoto, M. Minagawa, A. Tanioka, T. Danno, H. Horibe, Preparation of porous PVDF nanofiber from PVDF/PVP blend by electrospray deposition, *Polym. J.*, 39 (2007) 1060–1064.
- [25] C.Y. Lai, A. Groth, S. Gray, M. Duke, Preparation and characterization of poly(vinylidene fluoride)/nanoclay nanocomposite flat sheet membranes for abrasion resistance, *Water Res.*, 57 (2014) 56–66.
- [26] E. Pramono, M. Ahdiat, A. Simamora, W. Pratiwi, C.L. Radiman, D. Wahyuningrum, Surface properties and permeability of poly(vinylidene fluoride)-clays (PVDF/clays) composite membranes, *IOP Conf. Ser.: Earth Environ. Sci.*, 75 (2017) 012024.
- [27] L. Medjdoub, B. Mohammed, New method for nucleophilic substitution on hexachlorocyclotriphosphazene by allylamine using an Algerian proton exchanged montmorillonite clay (Maghnite-H⁺) as a green solid catalyst, *Bull. Chem. React. Eng. Catal.*, 11 (2016) 151–160.
- [28] I.Z. Mukasa-Tebandeke, P.J.M. Ssebuwufu, S.A. Nyanzi, A. Schumann, G.W.A. Nyakairu, M. Ntale, F. Lugolobi, The elemental, mineralogical, IR, DTA and XRD analyses characterized clays and clay minerals of Central and Eastern Uganda, *Adv. Mater. Phys. Chem.*, 5 (2015) 67–86.
- [29] C.-C. Chang, J.-H. Lin, L.-P. Cheng, Preparation of solvent-dispersible nano-silica powder by sol-gel method, *J. Appl. Sci. Eng.*, 19 (2016) 401–408.
- [30] E. Prasetyo, K. Toyoda, Sol-gel synthesis of a humic acid-silica gel composite material as low-cost adsorbent for thorium and uranium removal, *J. Radioanal. Nucl. Chem.*, 47 (2016) 69–80.
- [31] N. Minju, P. Abhilash, B.N. Nair, A. Peer Mohamed, S. Ananthakumar, Amine impregnated porous silica gel sorbents synthesized from water-glass precursors for CO₂ capturing, *Chem. Eng. J.*, 269 (2015) 335–342.
- [32] M. Besbes, N. Fakhfakh, M. Benzina, Characterization of silica gel prepared by using sol-gel process, *Phys. Procedia*, 2 (2009) 1087–1095.
- [33] T. Ogoshi, Y. Chujo, Synthesis of poly(vinylidene fluoride) (PVDF)/silica hybrids having interpenetrating polymer network structure by using crystallization between PVDF chains, *J. Polym. Sci. Part A Polym. Chem.*, 43 (2005) 3543–3550.
- [34] J.-Y. Lee, S. Qi, X. Liu, Y. Li, F. Huo, C.Y. Tang, Synthesis and characterization of silica gel-polyacrylonitrile mixed matrix forward osmosis membranes based on layer-by-layer assembly, *Sep. Purif. Technol.*, 124 (2014) 207–216.
- [35] J.-Y. Lee, Y. Wang, C.Y. Tang, F. Huo, Mesoporous silica gel-based mixed matrix membranes for improving mass transfer in forward osmosis: effect of pore size of filler, *Sci. Rep.*, 5 (2015) 1–9, doi: 10.1038/srep16808.
- [36] T. Marino, F. Russo, L. Rezzouk, A. Bouzid, A. Figoli, PES-kaolin mixed matrix membranes for arsenic removal from water, *Membranes (Basel)*, 7 (2017) 57, doi: 10.3390/membranes7040057.
- [37] D. Mondal, M.M.R. Mollick, B. Bhowmick, D. Maity, M.K. Bain, D. Rana, A. Mukhopadhyay, K. Dana, D. Chattopadhyay, Effect of poly(vinyl pyrrolidone) on the morphology and physical properties of poly(vinyl alcohol)/sodium montmorillonite nanocomposite films, *Prog. Nat. Sci.: Mater. Int.*, 23 (2013) 579–587.
- [38] M. Kobayashi, K. Tashiro, H. Tadokoro, Molecular vibrations of three crystal forms of poly(vinylidene fluoride), 8 (1975) 158–171.
- [39] A. Benaissa, S. Cheloufi, T. Etienne, S. Gasmi, Effect of stretching temperature on the structure and microstructure of poly(vinylidene fluoride), *Ann. Chim. Des Mater.*, 32 (2007) 615–631.
- [40] Q.-Y. Peng, P.-H. Cong, X.-J. Liu, T.-X. Liu, S. Huang, T.-S. Li, The preparation of PVDF/clay nanocomposites and the investigation of their tribological properties, *Wear*, 266 (2009) 713–720.
- [41] L. Yang, J. Qiu, K. Zhu, H. Ji, Q. Zhao, M. Shen, S. Zeng, Effect of rolling temperature on the microstructure and electric properties of β -polyvinylidene fluoride films, *J. Mater. Sci.: Mater. Electron.*, 29 (2018) 15957–15965.
- [42] M. Chakib Baghdadli, M. Belbachir, Acid-activated Algerian montmorillonite as heterogeneous catalysts for cationic polymerization of styrene, *Artic. Asian J. Chem.*, 28 (2016) 1197–1204.
- [43] W.K.W. Lee, J.S.J. van Deventer, Use of infrared spectroscopy to study geopolymerization of heterogeneous amorphous aluminosilicates, *Langmuir*, 19 (2003) 8726–8734.
- [44] H. Ajari, B. Chaouachi, F. Galiano, T. Marino, F. Russo, A. Figoli, A novel approach for dissolving crystalline LDPE using non-toxic solvents for membranes preparation, *Int. J. Environ. Sci. Technol.*, 16 (2019) 5375–5386.
- [45] Q.A. Bhatti, M.K. Baloch, S. Schwarz, G. Petzold, Impact of various parameters over the adsorption of polyvinylpyrrolidone onto kaolin, *J. Dispersion Sci. Technol.*, 33 (2012) 1739–1745.
- [46] F. Russo, T. Marino, F. Galiano, L. Gzara, A. Gordano, H. Organji, A. Figoli, S.M. Husson, Tamisolve® NxG as an alternative non-toxic solvent for the preparation of porous poly(vinylidene fluoride) membranes, *Membranes (Basel)*, 13 (2021) 2579, doi: 10.3390/polym13152579.
- [47] C. Ursino, F. Russo, R.M. Ferrari, M.P. De Santo, E. Di Nicolò, T. He, F. Galiano, A. Figoli, Polyethersulfone hollow fiber membranes prepared with Polarclean® as a more sustainable solvent, *J. Membr. Sci.*, 608 (2020) 118216, doi: 10.1016/j.memsci.2020.118216.
- [48] M. Chabane, C. Melkaoui, B. Dahmani, Z. Boudjenane, Influence of sodium maghnite nanoclay on the polyvinylidene fluoride crystal transition in composite membranes and its effect on bovine serum albumin protein extraction date de publication 2021/7/8, *Ann. Chim. Des Matériaux, Lavoisier*, 5 (2021) 191–200.